Photo-electrochemical behavior of CIGS solar thin films prepared through a novel CISe/Ga-Se two–step electrochemical stack approach

Ramkumar C, Archana Mallik*
Electrometallurgy and Corrosion Laboratory, Dept. of Metallurgical and Materials Engineering, NIT Roukele – 769008, India
archananitrkl@gmail.com

Abstract

Copper indium selenide ($CuInSe_2$ or CIS) thin films were electrodeposited on FTO substrates by co-electrodeposition of Cu-In-Se precursor thin films using an electrolyte comprised of Citric acid-SDS. By the addition of SDS, the formation of CIS nanoislands were avoided which can create compositional non-uniformity. They were further annealed at 400 ˚C in nitrogen atmosphere. The structural, compositional, optical and electronic characterization of as-deposited and annealed CIS thin films were investigated by XRD, Raman, FE-SEM/EDAX, UV-VIS spectroscopy and electrochemical analysis. With an optical bandgap of approximately 1 eV, the annealed CIS thin film exhibited a p-type behavior with excellent photoelectrochemical properties.

1. Introduction

$CuInSe_2$ (CIS) is an attractive direct bandgap (1.04 eV) semiconductor of second generation solar cells with high optical absorption coefficient ($\alpha=10^5$ cm^{-1}) and excellent optoelectronic stability can be fabricated either by vacuum or non-vacuum based techniques[1,2]. Till date, most of the high efficiency CIS/CIGS devices reported is fabricated by vacuum based techniques [3]. When compared to vacuum techniques, non-vacuum techniques such as electrodeposition, spray pyrolysis, chemical synthesis [4] are attractive as it has the potential to reduce the device fabrication cost drastically. Recently, a record efficiency of 15.9% for lab scale and a module efficiency of 12.2% were reported for CIGS thin film solar cells by Nexcis through electrodeposition approach [5]. Furthermore, electrodeposition is simple, cost effective, less material wastage and is industrially scalable for fabricating large area thin film solar cells. The ternary CISe thin films can electrodeposited by two approaches a) single step in which all the three elements are co-deposited by applying a single potential b) by stack approach ; electrodepositing Cu/In bilayer or Cu-In alloy followed by annealing in selenium atmosphere to obtain a uniphasic crystallinity CIS thin films [6,7]. Though single step deposition is appealing than stack approach due to its simplicity, the difference in the standard reduction potential of Cu^{2+} (-0.342/SHE), In^{3+} (-0.529/SHE) and Se^{4+} (+0.741/SHE) makes co-deposition of CIS difficult[8]. Controlling the Cu content in CIS is also challenging as the presence of excess Cu can form detrimental Cu_xSe secondary phase which acts as recombination centers and thus lowers the device performance in CIS thin films devices. As a post-processing step, Cu-rich absorber thin films either require selective etching (using KCN^-) to remove the excess Cu-content or a thin layer of Indium is to be deposited to make the surface Cu-poor[9]. Another common problem faced in co-deposition of CIS is the formation of pinholes due to the parallel occurrence of hydrogen evolution at higher co-deposition potential. Eliminating these

convolutions will help in obtaining a high photovoltaic quality CIS thin film with reduced pinholes and also we have the possibility to avoid the selenization step. As a step to eliminate these issues, we used have used a novel bath consisting of citric acid as the pH adjuster and sodium dodecyl sulfate (SDS) an anionic surfactant as the additive helps towards controlling the Cu-content, enhancing the Indium content and to reduce surface non-uniformities and pinholes[10].

In this research, we report our preliminary results pertaining to the characterization of CIS thin films deposited using Citrate-SDS electrolyte. The as-deposited and annealed CIS thin films were subjected to FESEM/EDAX, XRD, Raman and PEC studies to analyze the structure, morphology and electronic conductivity type.

2. Experimental

The deposition bath electrolyte was prepared by using chloride salts of $CuCl_2$ – 3.7 mM and $InCl_3$ – 5 mM along with H_2SeO_3 - 6 mM for the Selenium ions. The final pH of the bath was maintained at 1.8 by using citric acid. A well cleaned FTO coated glass substrates (1 x 0.5 cm^2) was used as the substrates and platinum foil as the counter electrode. For improving the as-deposited film compactness SDS of 21 mM was used as surfactant. To enhance the electrical conductivity, 0.15 gm of lithium chloride (LiCl) was added. All the electrochemical studies and deposition were performed in CorrTest Potentiostat. All the samples were electrodeposited at – 0.65 V for 20 minutes. The as-deposited films were then annealed in N_2 atmosphere at 400 °C for 20 min.

Results and Discussion

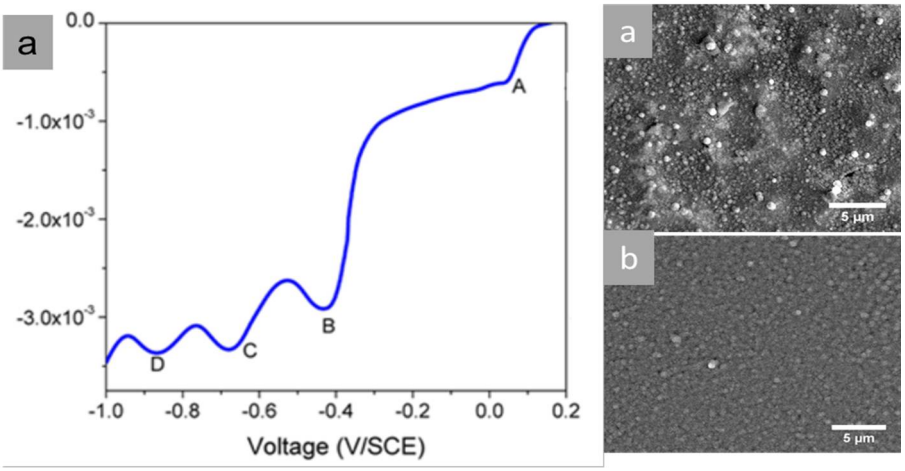

Fig.1 a) LSV of ternary Cu-In-Se ions in Citric acid and SDS electrolyte, b,c) FE-SEM of CIS deposited at -0.65 V/SCE for 20 min without SDS and with SDS (c)

Fig.1a shows the LSV of solution containing Cu, In and Se ions in citrate-SDS electrolyte. There are four prominent peaks observed between 0.20 to -1 V/SCE. The reduction peak A between 0 to -0.20 V can be assigned to the reduction of Cu^{2+} to Cu^0 according to Eqn. (1).

$$Cu^{2+} + 2e^- \rightleftarrows Cu \quad (1)$$

The onset of the reduction peak B can be assigned to the formation of Cu_2Se phase along with elemental Se(0) according to Eqn. (2) which is confirmed by the Raman studies provided in Fig.S1. According to Roussel et.al. the Cu_2Se phase along with excess elemental selenium can coexist as $CuSe_2$[11].

$$Se(IV) + 2Cu^0 + 4e^- \rightleftarrows Cu_2Se \quad (2)$$

Around -0.4 V (B), the indium inclusion taking place by surface induced reaction is often limited due to the increased electrical resistance of the surface due to the presence of Se(0) over the CuSe platelets according to Eqn.(3) [12,13].

$$CuSe_2 + 3In(III) + 3e^- \rightleftarrows CuInSe_2 \quad (3)$$

At higher cathodic potential (C), the Cu_2Se and Se(0) can undergo reduction to form Cu and H_2Se according to Eqn. (4-5). The formed H_2Se species chemically reacts with In^{3+} ions to form indium selenides (In_2Se_3) and assimilates to the growing $CuInSe_2$ film according to Eqn.(6).

$$Cu_2Se + 2H^+ + 2e^- \rightleftarrows Cu + H_2Se \quad (4)$$

$$Se + 2H^+ + 2e^- \rightleftarrows H_2Se \quad (5)$$

At higher cathodic potential (D), the In^{3+} ions can reduce to Indium according to Eqn. (7)[14]

$$Cu_2Se + 3H_2Se + 2In^{3+} \longrightarrow 2CuInSe_2 + 6H^+ \quad (6)$$

$$In^{3+} + 3e^- \rightleftarrows In \quad (7)$$

From the LSV results, the optimal deposition potential was fixed at -0.65 V/SCE for 20 min. After electrodeposition, the sample was washed with DI water, flushed with N_2 air to remove the water droplets and dried. To confirm the effect of pre-treatment (PT), FE-SEM studies were carried for the CIS thin films deposited with and without PT as shown in fig. 1b, c.

The sample deposited without SDS (Fig.1b) shows a rough grain distribution where the upper layer was found to be composed of multinuclear a spherical nanoisland which is undesirable for the device performance. The presence of these nano islands can alter the local Cu/In ratio during the annealing process and thus affect the compositional uniformity and reproducibility of the film. After the addition of SDS, the surface non-uniformities and nano-islands were minimized and the morphology was composed of densely packed smooth spherical grains (Fig.1c). The electrodeposition of CIS was carried at -0.65 V/SCE for 20 minutes. The obtained silvery grey CIS films were highly adherent to the FTO substrates. From EDAX analysis, the Cu/In ratio was determined to be 0.96 with the [Se/Cu+In] = 1.06. They were annealed subsequently in nitrogen atmosphere and used for further analysis.

Structural studies

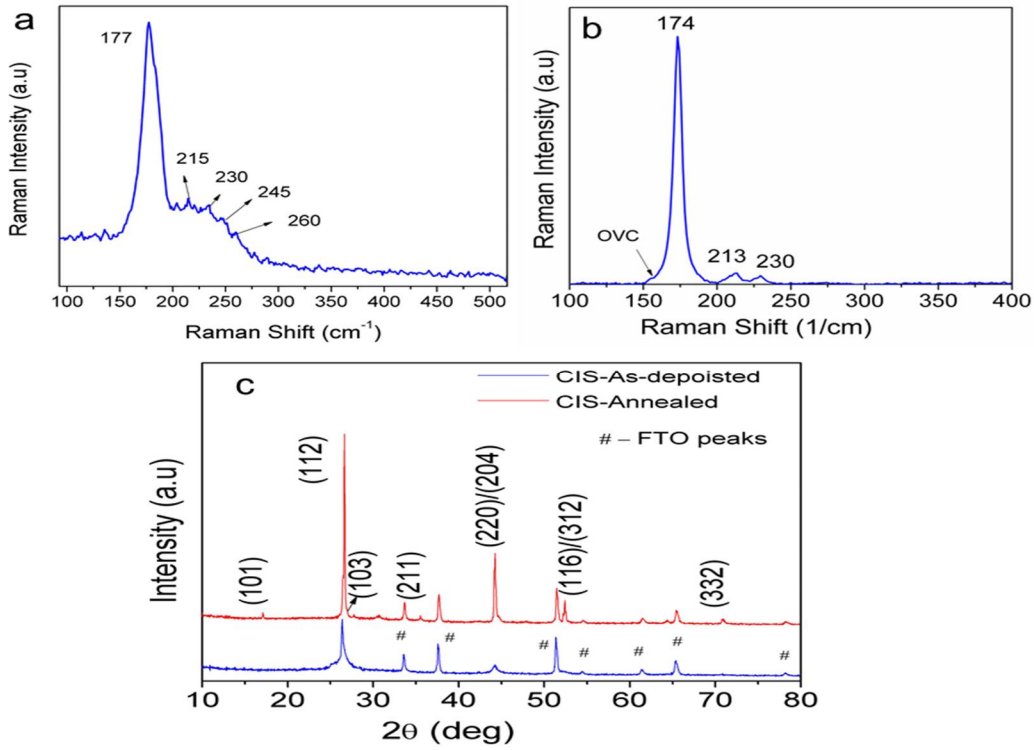

Fig.2 (a,b) shows the Raman spectra of as-deposited and annealed CIS thin films obtained using an excitation wavelength of 532 nm. The dominant peaks for as-deposited films were observed to be around 177, 215, 230, 245 and 260 cm^{-1} respectively. For a comprehensive understanding the peaks were deconvoluated and fitting was performed by lorentian method. The dominant peak at 177 cm^{-1} is generally observed in as-deposited I–III–VI_2 chalcopyrite compounds which can be assigned to the chalcopyrite A1 mode[11]. The wavenumbers at 215 and 230 cm^{-1} corresponds to the B2 and E modes of the chalcopyrite CIS. The peak at 240 cm^{-1} confirms the presence of trigonal elemental Se(0). The peak at 260 cm^{-1} corresponds to the Cu-Se impurity phase in un-annealed films[15]. Upon annealing, only 3 dominant peaks positioned at 174, 213 and 230 cm^{-1} can be observed (Fig.2b). A shoulder peak around 158 cm^{-1} for the annealed CIS films can be assigned to the Cu poor ordered vacancy compounds (OVC) which is a Cu-poor chalcopyrite with an average composition represented as $CuIn_3Se_5$ or $CuIn_5Se_8$ [16]. The red shift in the A1 (A1-3 cm^{-1}) mode towards the lower wavenumber 174 cm^{-1} suggest that during annealing, the stress release along with phase formation took place which is evident by the disappearance of elemental Se (0) and Cu-Se phase.

The XRD of as-deposited and annealed CIS films are shown in fig.2c. The strong preferential orientation of the (112) plane at 2θ= 26.6° indicates the improved crystallinity of the annealed CIS films along with minimal existence of secondary phase such as Cu-Se and In-Se which is in

agreement with the Raman studies. The presence of characteristic peaks corresponding to (101), (103), (211) etc., confirms the chalcopyrite phase as these phases are absent in sphalerite structure[17]. The diffraction peaks corresponding to annealed CIS films were matched with the JCPDS card No: 40-1487. The average grain size of the annealed CIS thin films were calculated using Scherrer's Formula as given in eqn (1)

Fig. 2 Raman spectra of as-deposited annealed CIS thin films (a, b), XRD of as-deposited and annealed CIS thin film (c)

$$Dp = \frac{K\lambda}{B\,Cos\theta} \text{ ---- (1)}$$

Where, D_p - Average crystallite size (nm), K - Scherrer constant. Usually the constant 'K' varies from 0.68 to 2.08. We have assumed K to be 0.94 for spherical crystallites, λ - X-ray wavelength, Cu Kα average = 1.54178 Å, B - FWHM (Full Width at Half Maximum) of XRD peak and θ - the XRD peak position, one half of 2θ. Using the above formula, we have calculated the crystallite size of annealed CIS films for 3 major diffraction peaks corresponding for the miller indices of (112), (204) and (312) planes. The calculated average crystallite size (Average Dp) estimated was around 37 nm. When considering only (112) plane, the crystallite size was calculated to be 72 nm.

Optical and Electrochemical impedance studies

Fig.3a shows the optical absorption coefficient plot determined from the UV-Vis absorbance spectra measured between the wavelength regions of 400-800 nm for as-deposited and annealed CIS thin films. For the determination of bandgap, a plot $(\alpha h\nu)^2$ vs. hν was constructed using the Tauc's relation provided in eqn. (2), where α- is the absorption coefficient, hν is the radiant energy, A-constant and E_g is the optical bandgap.

$$(\alpha h\nu)^2 = A_a(h\nu - E_g) \text{ -- (2)}$$

By extrapolation as shown in fig.3a, we can obtain an intercept of the straight line with the photon energy axis which can yield the optical band gap of CIS thin films. The bandgap for as-deposited and annealed CIS thin films were determined to be 1.25 eV and 1.09 eV respectively. The enhanced crystallinity, reduced defect states and phase formations may be attributed as the plausible explanations for the decrease in the optical bandgap values after annealing. The obtained values bandgap for annealed CIS was found to be in good agreement with the values reported by Haung *et al.*[18].

In Fig.3b, the EIS were performed for as-deposited and annealed CIS thin films in 0.5 M Na_2SO_4 solution to understand the charge transfer mechanism under illumination conditions. For this purpose, a conventional 100 W white light was used. The obtained Nyquist plot under illumination was fitted by using a Randles-Elsher type equivalent circuit (Fig.3b inset) with Warburg impedance to compute the charge transfer resistance (Rct) values with high accuracy[19].

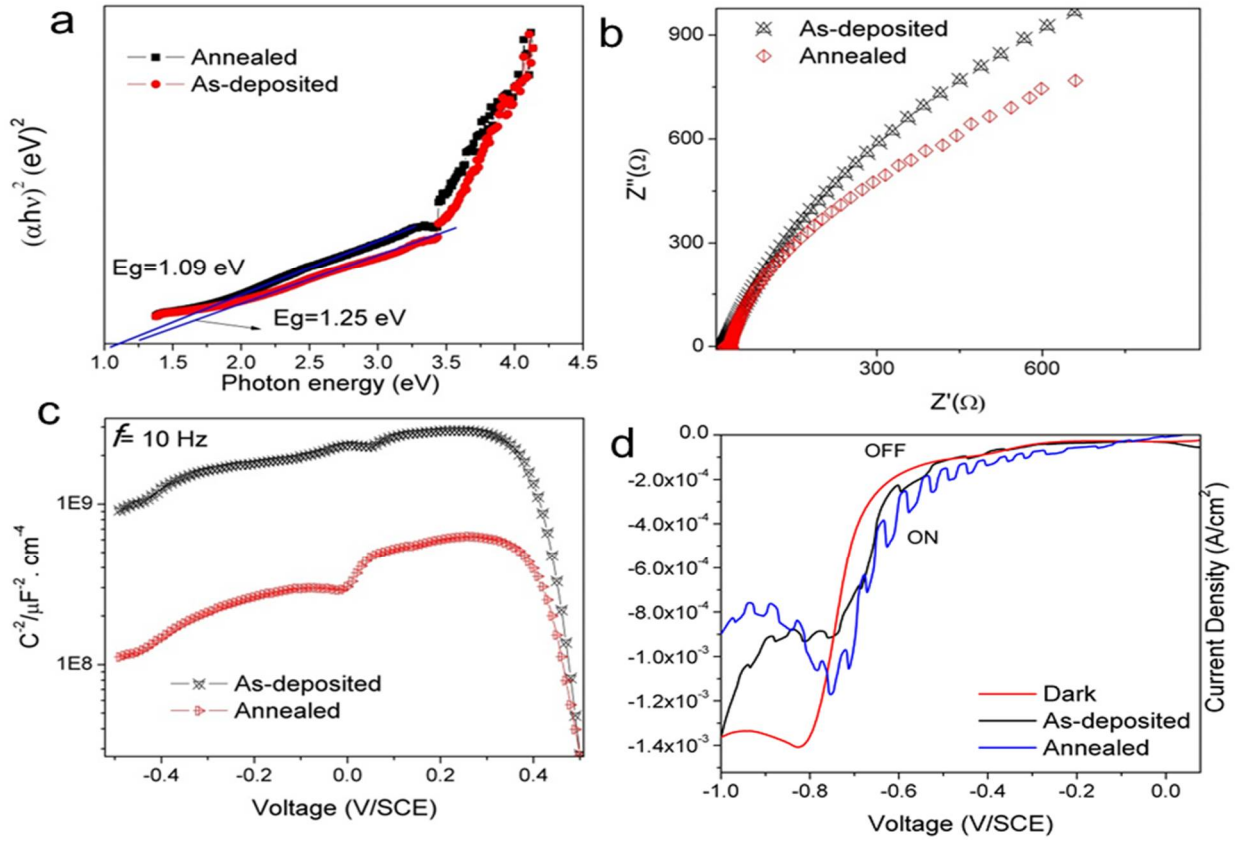

Fig.3 Plot of $(\alpha hv)^2$ vs. photon energy (a), Impedance spectra measured at -0.40 V/SCE (under illumination) (b,c) and M-S analysis (d) for as-deposited and annealed CIS thin films

The origin of the low series resistance around 33 Ω.cm^2 is due to the electrolyte resistance. The observed Rct values are 4609 and 1255 Ω.cm^2 for as-deposited and annealed CIS thin films respectively. Low Rct values imply that the annealed samples exhibited good interfacial charge transfer resistance with better electrical conductivity. The differential capacitance is measured as a function of potential for the CIS thin films in Na_2SO_4 alkaline electrolyte. The measurements were performed by applying an AC signal of 10 mV in the same working electrolyte used for deposition. The working frequency was fixed to be 10 Hz (estimated from the impedance studies).

$$\frac{1}{C^2} = \frac{2}{e\varepsilon\varepsilon_0 N_a}(V - Vfb - \frac{KT}{e}) \text{ -- (3)}$$

The Mott-Schottky (M-S) graph was plotted as shown in fig.4c based on the Eqn. (3), where C is the space charge capacitance, e – electronic charge (1.602×10^{-19} C), ε- dielectric constant of CIS (13.5), ε_0 - permittivity of free space (8.85×10^{-14} F.cm^{-1}), N_A or N_D is the hole (electron) acceptor (donor) concentration of the p (n) type semiconductor-applied potential w.r.to SCE, Vfb- flat band potential , k = Boltzmann constant (1.38×10^{-23} J.K^{-1}) and T is the temperature.

Table 1: Parameters extracted from Mott-schottky measurement of CIS thin films

Sample Name	Carrier concentration (cm^{-3})	Flatland potential (V/SCE)	Conductivity type
As-deposited	6.80×10^{16}	480 mV	P
Annealed	1.51×10^{16}	510	P

The negative slope feature observed in the differential capacitance curves indicates the p-type electrical conductivity of the CIS thin films. From the slope and intercept values of the M-S plot, the carrier concentration and flat band values were determined (table.1). The measured doping concentration of the as-deposited and annealed CIS thin films is found to be in closest match with the N_A values reported for the record efficiency devices [20,21]. The decrease in the doping concentration can be attributed to the stoichiometric changes which took place after annealing. The flat band potential (Vfb) was found to be decreasing with the increasing carrier concentration (N_A) and hence exhibits an inverse relationship. The larger Vfb values provide better driving force for the photogenerated charge carrier in the space charge region and hence enhance the power conversion efficiency.

To corroborate this, PEC studies were performed for the as-deposited and annealed CIS thin films in 0.5 M Na_2SO_4 electrolyte (Fig.3d). The reduced dark current features indicate the presence of minimal Cu_xSe secondary phase. The as-deposited CIS thin films showed a weak p-type behavior which is evident from the increasing cathodic current during illumination. The photo-activity improved after the post-annealing treatment. At a potential of -0.55 V/SCE, the obtained photocurrent density is 3.20 $x10^{-4}$ $A.cm^{-2}$ which is 55% higher than that of the as-deposited samples (2.069 $x10^{-4}$ $A.cm^{-2}$). The observed photocurrent values indicate the interdependence of the flat band potential and carrier concentration with the photoactivity of the CIS thin films.

Conclusion

The annealing effect on the electrodeposited CIS thin film using citrate-SDS electrolyte was studied. The addition of SDS have reduced the multinuclear outward growth and effectively eliminated the Cu-Se secondary phase which is detrimental to the device performance. Upon annealing, we were able to obtain crystalline, p-type uniphasic chalcopyrite CIS thin films with a bandgap of 1 eV. Finally, the photoelectrochemical properties of CIS thin films was found to be improved after annealing which is confirmed by the photo induced electrochemical I-V and impedance studies.

Acknowledgement:

The authors would like to thank NIT-Rourkela for providing the infrastructure and experimental facilities.

References:

[1] R.N. Bhattacharya, M.-K.K. Oh, Y. Kim, CIGS-based solar cells prepared from electrodeposited precursor films, Solar Energy Materials and Solar Cells. 98 (2012) 198–202. doi:10.1016/j.solmat.2011.10.026.

[2] N. Stratieva, E.M. Tzvetkova Ganchev K Kochev I Tomov, E. Tzvetkova, M. Ganchev, Structural

and optical properties of electrodeposited CuInSe 2 layers, Solar Energy Materials .... 45 (1997) 87–96. http://www.sciencedirect.com/science/article/pii/S0927024896000700 (accessed May 31, 2015).

[3] R. Chandran, S.K. Panda, A. Mallik, A short review on the advancements in electroplating of CuInGaSe2 thin films, Materials for Renewable and Sustainable Energy. 7 (2018) 6. doi:10.1007/s40243-018-0112-1.

[4] J. Ramanujam, U.P. Singh, Copper indium gallium selenide based solar cells – a review, Energy & Environmental Science. 10 (2017) 1306–1319. doi:10.1039/C7EE00826K.

[5] C. Broussillou, C. Viscogliosi, A. Rogee, S. Angle, P.P. Grand, S. Bodnar, et al., Statistical Process Control for Cu(In,Ga)(S,Se)2 electrodeposition-based manufacturing process of 60×120cm2 modules up to 14,0% efficiency, 2015 IEEE 42nd Photovoltaic Specialist Conference, PVSC 2015. (2015) 1–5. doi:10.1109/PVSC.2015.7356224.

[6] M.-H. Yeh, S.-J. Ho, G.-H. Chen, C.-W. Yeh, P.-R. Chen, H.-S. Chen, Toward low-cost large-area CIGS thin film III: Effect of Se concentration on crystal growth and defect formation of sequentially electrodeposited CIGS thin films, Solar Energy. 132 (2016) 547–557. doi:10.1016/j.solener.2016.03.029.

[7] P. Prosini, M. Addonizio, A. Antonaia, S. Loreti, Electrodeposition of copper-indium alloy under diffusion-limiting current control, Thin Solid Films. (1996). http://www.sciencedirect.com/science/article/pii/S0040609096088177 (accessed May 28, 2015).

[8] R. Chandran, C.K.Behera, A. Mallik, Electrochemical Impedance (EIS) behavior of CuInSe 2 (CIS) thin films on high resistance ITO/PET flexible substrates, Materials Today: Proceedings. 4 (2017) 12473–12479. doi:10.1016/j.matpr.2017.10.046.

[9] V. Deprédurand, D. Tanaka, Y. Aida, M. Carlberg, N. Fèvre, S. Siebentritt, Current loss due to recombination in Cu-rich CuInSe2 solar cells, Journal of Applied Physics. 115 (2014) 044503-8. doi:10.1063/1.4862181.

[10] A.M. Chandran Ramkumar, Rajneesh Pandey, R. Chandran, R. Pandey, A. Mallik, A.M. Chandran Ramkumar, Rajneesh Pandey, R. Chandran, et al., One step electrodeposition of CuInSe2 from an acidic bath: A reduction CO-deposition study, Materials Letters. 160 (2015) 275–277. doi:10.1016/j.matlet.2015.07.132.

[11] O. Roussel, O. Ramdani, E. Chassaing, P.-P. Grand, M. Lamirand, A. Etcheberry, et al., First Stages of CuInSe[sub 2] Electrodeposition from Cu(II)-In(III)-Se(IV) Acidic Solutions on Polycrystalline Mo Films, Journal of The Electrochemical Society. 155 (2008) D141. doi:10.1149/1.2815476.

[12] P. Carbonnelle, L. Lamberts, A voltammetric study of the electrodeposition chemistry of the Cu + Se system, Journal of Electroanalytical Chemistry. 340 (1992) 53–71. doi:10.1016/0022-0728(92)80289-G.

[13] M.E. Calixto, K.D. Dobson, B.E. McCandless, R.W. Birkmire, Growth Mechanisms of Electrodeposited CuInSe2 and Cu(In,Ga)Se2 Determined by Cyclic Voltammetry, MRS Proceedings. 865 (2005) F14.17. doi:10.1557/PROC-865-F14.17.

[14] Y. Lai, J. Liu, J. Yang, B. Wang, F. Liu, Z. Zhang, et al., Incorporation Mechanism of Indium and

Gallium during Electrodeposition of Cu(In,Ga)Se2 Thin Film, Journal of The Electrochemical Society. 158 (2011) D704. doi:10.1149/2.059112jes.

[15] O. Ramdani, J.F.F. Guillemoles, D. Lincot, P.P.P. Grand, E. Chassaing, O. Kerrec, et al., One-step electrodeposited CuInSe2 thin films studied by Raman spectroscopy, Thin Solid Films. 515 (2007) 5909–5912. doi:10.1016/j.tsf.2007.02.109.

[16] V. Izquierdo-Roca, E. Saucedo, C.M. Ruiz, X. Fontané, L. Calvo-Barrio, J. Álvarez-Garcia, et al., Raman scattering and structural analysis of electrodeposited $CuInSe_2$ and S-rich quaternary $CuIn(S,Se)_2$ semiconductors for solar cells, Physica Status Solidi (A). 206 (2009) 1001–1004. doi:10.1002/pssa.200881239.

[17] S.R. Kodigala, Thin film and nanostructures Cu(In1_xGax)Se2 Based Thin Film Solar Cells, 2000. doi:1543-5016.

[18] C.J. Huang, T.H. Meen, M.Y. Lai, W.R. Chen, Formation of CuInSe2 thin films on flexible substrates by electrodeposition (ED) technique, Solar Energy Materials and Solar Cells. 82 (2004) 553–565. doi:10.1016/j.solmat.2003.12.008.

[19] A. Lasia, Electrochemical Impedance Spectroscopy and its Applications, Modern Aspects Of Electrochemistry. 32 (1999) 143–248. doi:10.1007/0-306-46916-2_2.

[20] J.A.M. AbuShama, S. Johnston, T. Moriarty, G. Teeter, K. Ramanathan, R. Noufi, Properties of ZnO/CdS/CuInSe2 solar cells with improved performance, Progress in Photovoltaics: Research and Applications. 12 (2004) 39–45. doi:10.1002/pip.537.

[21] P. Jackson, D. Hariskos, R. Wuerz, O. Kiowski, A. Bauer, T.M. Friedlmeier, et al., Properties of Cu(In,Ga)Se 2 solar cells with new record efficiencies up to 21.7%, Physica Status Solidi (RRL) - Rapid Research Letters. 9 (2015) 28–31. doi:10.1002/pssr.201409520.